

Coupled Charge-Spin Dynamics of the Magnetoresistive Pyrochlore $\text{Ti}_2\text{Mn}_2\text{O}_7$ Probed Using Ultrafast Midinfrared Spectroscopy

R. P. Prasankumar,^{1,*} H. Okamura,² H. Imai,³ Y. Shimakawa,³ Y. Kubo,³ S. A. Trugman,¹ A. J. Taylor,¹ and R. D. Averitt¹

¹*Los Alamos National Laboratory, Los Alamos, New Mexico 87545, USA*

²*Graduate School of Science and Technology, Kobe University, Kobe 657-8501, Japan*

³*Fundamental Research Laboratories, NEC Corporation, Tsukuba 305-8501, Japan*

(Received 17 December 2004; revised manuscript received 5 October 2005; published 23 December 2005)

Optical-pump midinfrared probe spectroscopy is used to investigate coupled charge-spin dynamics in the magnetoresistive pyrochlore $\text{Ti}_2\text{Mn}_2\text{O}_7$. We find that the temporal persistence of the photoexcited carrier density is strongly influenced by spin disorder above and below the ferromagnetic Curie temperature. Our results are consistent with a picture whereby spin disorder leads to spatial segregation of the initially excited Tl $6s$ -O $2p$ electron-hole pairs, effectively reducing the probability for recombination. This further implies that colossal magnetoresistance in these materials may be driven primarily by Mn t_{2g} spin disorder.

DOI: 10.1103/PhysRevLett.95.267404

PACS numbers: 78.47.+p, 75.47.Gk

Colossal magnetoresistance (CMR) materials have received a great deal of attention in recent years. The best known example of these materials are the ferromagnetic perovskite manganites such as $\text{La}_{1-x}\text{Sr}_x\text{MnO}_3$ ($x \sim 0.3$) [1–3], in which the CMR mechanism is believed to originate from the combined effects of double exchange and Jahn-Teller distortions. The rich physics inherent to this class of materials, along with the potential for applications in many areas such as spintronics and magnetic data storage, has prompted a search for other compounds with similar properties.

The pyrochlore $\text{Ti}_2\text{Mn}_2\text{O}_7$ (TMO) exhibits a paramagnetic insulator to ferromagnetic metal transition and CMR near the Curie temperature $T_c \sim 120$ K comparable to that seen in the doped perovskites [4–6]. However, the CMR mechanism is expected to be very different in this compound since double exchange and Jahn-Teller (JT) effects are negligible due to the low carrier density and absence of the JT ion Mn^{3+} [4,5]. It is generally believed that separate subsystems are responsible for ferromagnetic ordering (Mn $3d$ electrons) and conduction (Tl $6s$ electrons) in TMO [5,7]. The ferromagnetic ordering of the Mn^{4+} sublattice below T_c likely occurs through superexchange interactions [5,8]. This ferromagnetic ordering strongly modifies the electronic states (through indirect exchange interactions), causing a minority spin band with primarily Tl $6s$ character to shift below the Fermi level (E_F) and creating a spin-polarized carrier density that is responsible for conduction [8–10] (Fig. 1). This is corroborated by Hall effect measurements that show a carrier density change from $0.8 \times 10^{19} \text{ cm}^{-3}$ in the paramagnetic insulating phase to $5 \times 10^{19} \text{ cm}^{-3}$ in the ferromagnetic conducting phase [11]. Optical conductivity experiments also reveal a transition from insulatorlike to metallic behavior as the temperature is tuned below T_c , with a corresponding Drude-like reflectivity plasma edge that shifts to higher energies [~ 0.1 eV—see Fig. 2(a)] as the carrier density increases [12]. This carrier density change has been considered as a

driving mechanism for CMR in TMO [11,12]. Another mechanism leading to CMR just above T_c , where the carrier density is very low, has also been proposed, based on the delocalization of magnetic polarons due to a reduction in spin scattering upon application of a magnetic field [7,13–15].

Ultrafast spectroscopy has contributed to understanding the perovskite manganites by differentiating between the relative contributions of the lattice and spin degrees of freedom in determining the electronic and transport properties [16–19]. Time-resolved measurements on manganite films revealed a scaling of the spin-lattice relaxation time with the magnetic specific heat [16,17,20]. It was found that thermally disordered phonons limit the hole transport at temperatures well below T_c , while spin fluctuations become more important as the temperature T increases towards T_c . Time-resolved measurements on other CMR materials should provide additional insight into the properties that drive CMR phenomena, making TMO particularly interesting.

In this Letter, optical-pump midinfrared (IR) probe spectroscopy is used to investigate the carrier dynamics in

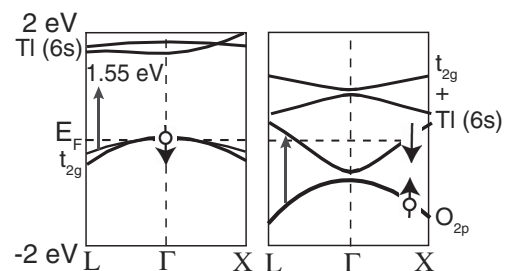


FIG. 1. Band structure of ferromagnetic (i.e., $T = 0$) $\text{Ti}_2\text{Mn}_2\text{O}_7$ near the Γ point, showing the majority (left) and minority (right) spin manifolds. The arrows label the 1.55 eV pump energy used in these experiments. Spin orientations for photoexcited quasiparticles in a $t_{2g}(\uparrow)$ domain are also shown.

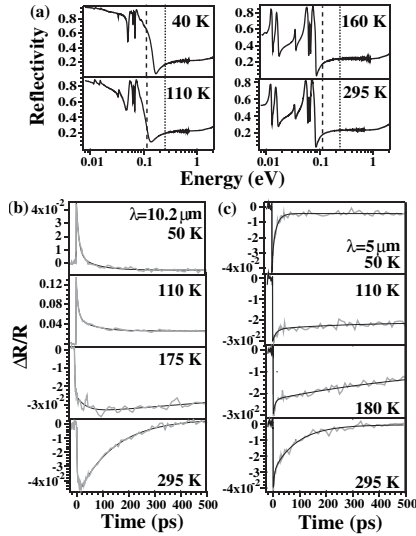


FIG. 2. (a) Reflectivity as a function of temperature and frequency [12]. The dashed line corresponds to the $10.2 \mu\text{m}$ probe wavelength, and the dotted line indicates the $5 \mu\text{m}$ probe wavelength. (b) Temperature dependent measurements on $\text{Tl}_2\text{Mn}_2\text{O}_7$ with a $10.2 \mu\text{m}$ probe. (c) Temperature dependent measurements on $\text{Tl}_2\text{Mn}_2\text{O}_7$ with a $5 \mu\text{m}$ probe.

TMO as a function of temperature. We show that the lifetime of the photoexcited carrier density is strongly influenced by spin disorder throughout the measured temperature range, with static Mn t_{2g} spin disorder (on the time scale of our experiments) dominating the dynamics for $T \leq 0.75T_c$, and thermal t_{2g} spin fluctuations dominating for $T \geq 1.4T_c$. In particular, spin disorder leads to spatial segregation of the initially excited Tl $6s$ -O $2p$ electron-hole pairs, effectively reducing the probability for recombination. Our results suggest that CMR in TMO may originate from spin disorder and further, that TMO may be a particularly simple example (i.e., low carrier density and no JT phonons) where the transport properties are determined by intrinsic nanoscale inhomogeneity occurring at a second order phase transition [21].

The TMO sample was synthesized by a high pressure solid state reaction and polished for optical measurements [4,12]. The measured Curie temperature is 120 K and the Curie-Weiss temperature is 175 K [8]. The optical-pump, mid-IR probe system is based on a 1 kHz regenerative amplifier producing 2 mJ, 60 fs pulses at 800 nm. The amplifier output is split into two beams to excite the sample and pump an optical parametric amplifier (OPA). The signal and idler beams from the OPA are mixed in a nonlinear crystal to generate the tunable 3–20 μm mid-IR probe [22]. The probe energy was $< 1\%$ of the pump energy in all experiments.

The measurements were performed in reflection at near normal incidence with the pump and probe s polarized and a pump wavelength of 800 nm (1.55 eV) used to excite the sample. This choice of pump energy is important since, as indicated in Fig. 1, 1.55 eV photons selectively excite

electrons into the minority spin manifold (the energy gap in the majority spin manifold is ~ 2 eV) [8–10]. Thus, we photoexcite electrons into the band that is responsible for conduction in TMO, allowing us to subsequently probe the dynamics of the free carrier response (more detail is provided below). Probing at midinfrared frequencies is critical, as the largest temperature dependent changes in the time-integrated reflectivity spectrum occur in this wavelength range [Fig. 2(a)]. Temperature dependent measurements with a $10.2 \mu\text{m}$ (0.12 eV) probe are shown in Fig. 2(b). The pump fluence was $460 \mu\text{J}/\text{cm}^2$, exciting an initial carrier density of $2.4 \times 10^{20} \text{ cm}^{-3}$. Figure 2(c) depicts measurements with a $5 \mu\text{m}$ (0.25 eV) probe; the pump fluence was $740 \mu\text{J}/\text{cm}^2$, exciting an initial carrier density of $4.2 \times 10^{20} \text{ cm}^{-3}$.

At all temperatures and probe wavelengths, the traces show a rapid change in reflectivity at zero delay, followed by a fast relaxation with a time scale of a few picoseconds and a slower component with a time scale of tens to hundreds of picoseconds. The sign of the pump induced normalized change in reflectivity, $\Delta R/R$, at probe wavelengths of 5 and $10.2 \mu\text{m}$ is consistent with a photoinduced increase in the carrier density, causing a shift of the plasma edge to higher energies. That is, $\Delta R/R \sim (1/R) \times (\partial R/\partial n)\Delta n$, where n is the carrier density and Δn the photoinduced increase in the carrier density. Using the time-integrated optical conductivity, we can accurately determine $(1/R)(\partial R/\partial n)\Delta n$ as a function of temperature for any Δn . This was accomplished by representing the dielectric constant with a sum of Lorentz phonon oscillators and a Drude term (Refs. [23,24]) and verified by fitting the reflectivity curves in Ref. [12]. At $10.2 \mu\text{m}$, the analysis predicts that $\Delta R/R$ should be positive at low temperatures and a crossover to negative $\Delta R/R$ should occur with increasing temperature, in agreement with the data in Fig. 2(b). The analysis also predicts that $\Delta R/R$ at $5 \mu\text{m}$ should be negative at all temperatures, again in agreement with experiment [Fig. 2(c)]. In short, our results are consistent with excitation of carriers from a low lying band of predominantly oxygen $2p$ character into the Tl $6s$ minority spin band that crosses the Fermi level (Fig. 1) [25].

There is a relatively temperature independent fast (~ 10 ps) initial relaxation in $\Delta R/R$ at $10.2 \mu\text{m}$, leaving fewer photoexcited carriers to contribute to the Drude-like response. Nearly all the carriers follow this recombination pathway for $T \ll T_c$. However, upon approaching T_c , the magnitude of the transient reflectivity signal increases significantly, both at $t = 0$ and at longer times ($t \geq 50$ ps), after the carriers have reached a thermal distribution. That is, a large offset appears in $\Delta R/R$ near and above T_c , indicating the establishment of a long-lived carrier population. Similar behavior is observed at $5 \mu\text{m}$, though the absolute magnitude of $\Delta R/R$ is smaller than that measured at $10.2 \mu\text{m}$. This is expected since the largest changes in the static reflectivity with carrier density occur near the plasma edge. In the following we present a more

detailed analysis which reveals a strong charge-spin coupling in TMO.

To obtain a more quantitative understanding of the charge and spin dynamics in TMO, we extracted $\Delta n(t, T)$ by using the previously described models for the dielectric constant and our $5 \mu\text{m}$ pump-probe data. We calculated the photoinduced carrier density at $t = 50$ and 500 ps [Fig. 3(a)]. In region 1 ($T \leq 90$ K), the photoinduced carrier density at both time delays is nearly identical, increasing as T approaches T_c . As T increases past T_c , $\Delta n(t = 500 \text{ ps})$ remains nearly constant in region 2 ($90 \text{ K} \leq T \leq 170 \text{ K}$) and then decreases rapidly in region 3 ($T \geq 170 \text{ K}$), completely disappearing by 295 K , while at $t = 50$ ps a significant fraction of carriers remain at 295 K .

We first focus on the evolution of the photoexcited carrier density with temperature in region 1. Energy considerations and dipole selection rules dictate that the pump excitation creates electron-hole ($e-h$) spin singlets in the minority spin manifold. At the lowest temperatures the $e-h$ singlets are created in a homogeneous background of t_{2g} spins [Fig. 4(a)]. Under these conditions, there is no energetic or dynamic constraint hindering recombination. That is, $e-h$ wave function overlap in a spin singlet configuration occurs with a high probability, leading to recombination and a fast recovery of the carrier density (<15 ps) as our data shows. However, with increasing temperature a long-lived carrier density develops [Fig. 3(a)]. This indicates that a competing pathway develops that stabilizes a fraction of the photoexcited carriers against recombination.

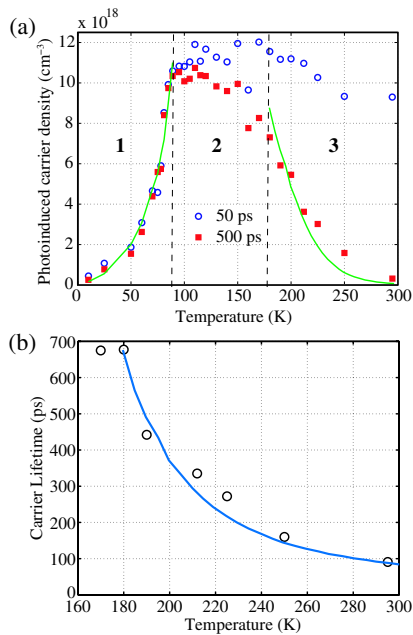


FIG. 3 (color online). (a) Photoinduced carrier density Δn at $t = 50$ ps (circles) and $t = 500$ ps (squares). The solid lines are fits as described in the text. (b) Carrier lifetime vs temperature for $T \geq 170$ K (circles). The solid line is the paramagnetic susceptibility, scaled to fit the plot [8].

A route for stabilizing a fraction of the initially photoexcited carriers is through the development of spatial fluctuations (with a characteristic length scale given by the magnetic correlation length $\xi(T)$) of the Mn t_{2g} spins responsible for ferromagnetic ordering. That is, small regions of opposite t_{2g} spin develop in an otherwise homogeneous background. This is schematically depicted in Fig. 4 where for $T \ll T_c$ [Fig. 4(a)] the density of $t_{2g}(\uparrow)$ domains is quite low but strongly increases upon approaching T_c [Fig. 4(b)]. Of course ξ is also temperature dependent (diverging at T_c as for any ferromagnet), but in region 1 ($T < 90$ K) $\xi \sim 1$ (i.e., ~ 0.1 nm) [26]. In this simple picture, we emphasize that it is therefore the density of “defects” of opposite t_{2g} orientation that capture the essential physics of carrier stabilization.

The spatial inhomogeneity that develops has important implications for photoexcited electron-hole pairs. From the band structure, it can be seen that it is energetically favorable for O $2p$ holes to cross a $t_{2g}(\uparrow)$ - $t_{2g}(\downarrow)$ boundary whereas there is an energetic barrier for the Tl $6s$ electrons. Thus, the spatial inhomogeneity in the t_{2g} spin manifold leads to spatial segregation of the photoexcited Tl $6s$ electrons and O $2p$ holes which, in turn, inhibits recombination. However, this process competes with recombination and spatial segregation can only occur for holes that are initially created within a distance λ of a boundary as depicted in Fig. 4. The net result is that with increasing temperature the number of defects increases, leading to an increase in the Tl $6s$ carrier density since more O $2p$ holes can be trapped.

Thus, in region 1, the amplitude of the fast component of the relaxation is due to recombination while the amplitude of the slow component is due to carrier stabilization as described above. Therefore, the photoinduced carrier density at $t = 500$ ps should be proportional to the ratio of slow to fast amplitudes in our $\Delta R/R$ traces (verified for our $5 \mu\text{m}$ probe data). This, in turn, scales with the ratio of the volume occupied by $t_{2g}(\uparrow)$ spins to that occupied by $t_{2g}(\downarrow)$

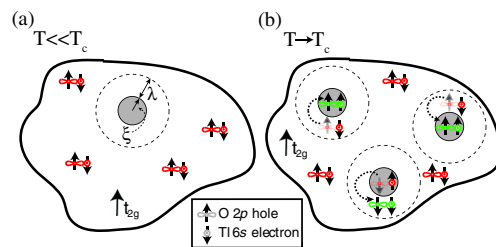


FIG. 4 (color online). (a) Photoexcited spin singlets for $T \ll T_c$. The gray shaded area is a domain with spin down t_{2g} states and the unshaded area is a domain with spin up t_{2g} states, with ξ and λ defined in the text. The electron-hole pairs recombine quickly in this temperature range. (b) Electron-hole pairs after photoexcitation as T approaches T_c from below. In this temperature range, holes within λ of a boundary migrate to domains of opposite t_{2g} spin orientation (dotted arrows), effectively preventing $e-h$ recombination.

spins, including a factor $\gamma = (\lambda + \xi)^3$. Here, γ is the effective volume where the probability of trapping an O $2p$ hole is greater than a recombination event. This results in an expression for the excess Tl $6s$ electron density Δn given by

$$\Delta n = C_0 \frac{\gamma(1 - M)}{2\xi^3 - \gamma(1 - M)}, \quad (1)$$

where the magnetization M is normalized to its saturation value and C_0 is a proportionality constant. We varied λ and C_0 to fit our data for $T < 90$ K, using $\xi = 1$ and the experimentally measured M [8]. The solid line in Fig. 3(a) shows Δn plotted as a function of temperature for $T < 90$ K, revealing excellent agreement with our data. This analysis also yields $\lambda \sim 0.79$ unit cells, indicating that the photoexcited holes can only travel a limited distance before recombining; this agrees well with the low hole mobility expected from the majority spin band structure (Fig. 1). In short, spatial inhomogeneity that develops in the t_{2g} spins (responsible for a decrease in M) stabilizes a fraction of the photoexcited carriers.

In region 2 (90–170 K), the concentration of Tl $6s$ electrons stabilized against recombination saturates [Fig. 3(a)]. Equation (1) is no longer valid, but some insight can be obtained regarding this saturation. At high temperatures the defects of volume γ begin to overlap which limits further increases in Δn at long times. Our simple model predicts that the temperature at which this saturation occurs depends on λ . For example, a larger hole mobility implies a larger λ (and γ) which would lead to saturation at a lower temperature. We also note that the extremely long lifetime of the excess electrons ($\gg 1.5$ ns) implies that the opposite spin t_{2g} defects are effectively static over the time scales measured.

However, in region 3 ($T \geq 170$ K), the concentration of photoexcited Tl $6s$ electrons remaining at 500 ps decreases with increasing temperature [Fig. 3(a)]. This indicates that the increase in thermal fluctuations of the t_{2g} spins effectively raises the probability for electron-hole wave function overlap and therefore the recombination rate. In fact, the recombination time τ of the photoexcited carrier density [as determined from exponential fits to the slow component of the data in Fig. 2(c)] scales with the paramagnetic susceptibility χ . This is shown in Fig. 3(b), where τ is plotted versus temperature along with the experimentally measured $\chi(T)$ (scaled to fit the plot) [8]. The recombination time decreases from 700 ps at 170 K to 100 ps at 295 K. The excellent agreement of this data shows that $\tau \sim \chi$ in region 3. We further verified this relation by calculating $\Delta n(t) = \Delta n(t=0)e^{-t/\tau}$ using the susceptibility data in Ref. [8]; the agreement with our data is depicted in Fig. 3(a) (solid line for $T \geq 170$ K). These results show that paramagnetic t_{2g} spin fluctuations determine the recombination time in TMO for temperatures above 170 K.

In conclusion, we have measured time-resolved carrier dynamics in $\text{Tl}_2\text{Mn}_2\text{O}_7$ for the first time. We find that the

carrier lifetime is linked to spin disorder throughout our measured temperature range. Quite generally, spin disorder opens a channel for spatial segregation of a fraction of the photoexcited Tl $6s$ -O $2p$ electron-hole pairs. This results in the development of a long-lived electron distribution with a Drude-like response since recombination is effectively suppressed. These results are consistent with CMR in $\text{Tl}_2\text{Mn}_2\text{O}_7$ arising from carrier localization due to strong spin fluctuations without invoking phonons. Our results also suggest that $\text{Tl}_2\text{Mn}_2\text{O}_7$ may be a particularly simple example where the transport properties are determined by intrinsic nanoscale inhomogeneity occurring near a second order phase transition.

We thank Cristian Batista for helpful suggestions. This research was supported by the Los Alamos LDRD program.

*Electronic address: rpprasan@lanl.gov

- [1] S. Jin *et al.*, *Science* **264**, 413 (1994).
- [2] A. Millis, *Nature (London)* **392**, 147 (1998).
- [3] *Colossal Magnetoresistive Oxides*, edited by Y. Tokura (Gordon and Breach, Amsterdam, 2000).
- [4] Y. Shimakawa, Y. Kubo, and T. Manako, *Nature (London)* **379**, 53 (1996).
- [5] M. A. Subramanian *et al.*, *Science* **273**, 81 (1996).
- [6] S.-W. Cheong, H. Y. Hwang, B. Batlogg, and L. W. Rupp, *Solid State Commun.* **98**, 163 (1996).
- [7] B. Martinez *et al.*, *Phys. Rev. Lett.* **83**, 2022 (1999).
- [8] Y. Shimakawa *et al.*, *Phys. Rev. B* **59**, 1249 (1999).
- [9] D. J. Singh, *Phys. Rev. B* **55**, 313 (1997).
- [10] S. K. Mishra and S. Satpathy, *Phys. Rev. B* **58**, 7585 (1998).
- [11] H. Imai, Y. Shimakawa, Y. V. Sushko, and Y. Kubo, *Phys. Rev. B* **62**, 12 190 (2000).
- [12] H. Okamura *et al.*, *Phys. Rev. B* **64**, 180409(R) (2001).
- [13] P. Majumdar and P. Littlewood, *Phys. Rev. Lett.* **81**, 1314 (1998).
- [14] P. Majumdar and P. B. Littlewood, *Nature (London)* **395**, 479 (1998).
- [15] P. Velasco *et al.*, *Phys. Rev. B* **66**, 174408 (2002).
- [16] R. D. Averitt *et al.*, *Phys. Rev. Lett.* **87**, 017401 (2001).
- [17] R. D. Averitt and A. J. Taylor, *J. Phys. Condens. Matter* **14**, R1357 (2002).
- [18] T. Ogasawara *et al.*, *J. Phys. Soc. Jpn.* **71**, 2380 (2002).
- [19] S. A. McGill *et al.*, *Phys. Rev. Lett.* **93**, 047402 (2004).
- [20] A. I. Lobad *et al.*, *Chem. Phys.* **251**, 227 (2000).
- [21] E. Dagotto, *Nanoscale Phase Separation and Colossal Magnetoresistance* (Springer, Berlin, 2003).
- [22] H. Maekawa, K. Tominaga, and D. Podenas, *Jpn. J. Appl. Phys.* **41**, L329 (2002).
- [23] F. Gervais *et al.*, *Phys. Rev. B* **47**, 8187 (1993).
- [24] N. E. Massa *et al.*, *Phys. Rev. B* **60**, 7445 (1999).
- [25] We have verified using the two temperature model that heating gives a negligible contribution to $\Delta R/R$ except at the lowest temperatures ($T < 50$ K) and that the sign of $\Delta R/R$ expected from heating is the opposite of our experimental observations.
- [26] J. W. Lynn, L. Vasiliu-Doloc, and M. A. Subramanian, *Phys. Rev. Lett.* **80**, 4582 (1998).